Available online at www.sciencedirect.com

ScienceDirect

Procedia Structural Integrity 33 (2021) 89–96

Structural Integrity Procedia

www.elsevier.com/locate/procedia

IGF26 - 26th International Conference on Fracture and Structural Integrity

Effect of graphene on the fracture behaviour of 3D printed PLA SENB specimens

Victor Martinez, Sergio Cicero*, Borja Arroyo.

LADICIM (Laboratory of Materials Science and Engineering), University of Cantabria, E.T.S. de Ingenieros de Caminos, Canales y Puertos, Av/Los Castros 44, 39005 Santander, Spain

Abstract

This paper analyses the effect of graphene addition on the fracture behaviour of 3D printed PLA SENB specimens containing crack-like defects. The addition of graphene is assumed to improve the tensile behaviour of 3D printed PLA material, but the integrity of structural components strongly depends on the material fracture resistance. Tensile and fracture SENB specimens have been tested with different raster orientations (0/90, 30/−60 and 45/−45), showing that the effect of graphene addition (1 wt. %) is very sensitive to the raster orientation: this effect is significant for raster orientation 45/-45 and very limited for 0/90 (with 30/-60 providing intermediate results).

Keywords: graphene; fracture behaviour.

1. Introduction

Additive manufacturing is a widely used fabrication process these days because it allows singular geometries to be created in an easy way. Several methods can be distinguished in this technology such as: material extrusion, material jetting, power bed fusion, binder jetting, vat photopolymerization, sheet lamination and directed energy deposition, fused deposition modelling (FDM) (material extrusion) being the most used. FDM consists in depositing

* Corresponding author. Tel.: 34-942-200-017
E-mail address: ciceros@unican.es

10.1016/j.prostr.2021.10.013

a wire material on the printing bed layer by layer until the desired geometry is obtained. The wire is previously melted and extruded in a nozzle. The full process is monitored by a software (Dwiyati et al., 2019).

Before the printing process, a number of different parameters have to be configured, such as raster orientation, infill level, layer height or printing temperature. It is widely reported in the literature that these parameters directly affect the mechanical properties of the resulting material (Fernandez-Vicente et al., 2016; Rodríguez-Panes et al., 2018; Samykano et al., 2019; Wu et al., 2015; Ziemian et al., 2012). Particularly, raster orientation has a great impact on the material resistance and will be studied in this paper (Afrose et al., 2014; Ayatollahi et al., 2020; Bamiduro et al., 2019; Jap et al., 2019; Rankouhi et al., 2016).

Polymers are the most common 3D-printed materials. Specifically, ABS (acrylonitrile butadiene styrene) and PLA (polylactic acid) are widely used j in this field. Materials are commonly combined with other elements (reinforcements) to obtain better properties, resulting in 3D-printed composites. One of the materials with a broad application as a reinforcement is graphene and its derivatives (e.g., graphene oxide). This material presents excellent mechanical properties that can improve the mechanical behaviour of the original matrix.

PLA and PLA reinforced with graphene (including 3D-printed materials) have been previously analysed in the literature, analysing the corresponding tensile properties (Afrose et al., 2014; Caminero et al., 2019; Marconi et al., 2018; Rodríguez-Panes et al., 2018). However, there are very few examples of works dealing with the fracture behaviour of these materials (e.g., Kiendl and Gao, 2020). For this reason, this paper analyses the fracture behaviour of 3D-printed PLA and PLA reinforced with graphene.

2. Materials and methods

This research analyses the fracture behaviour of 3D-printed PLA and 3D-printed PLA reinforced with graphene (PLA-GR) cracked specimens, evaluating the graphene effect as a reinforcement. PLA-GR contains a fixed amount of 1wt.% of graphene. Both materials, PLA and PLA-GR, were supplied by FiloAlfa3D (Milano, Italy).

In order to characterise both materials, an experimental programme was performed. A total of 24 fracture test and 30 tensile tests were carried out (12 fracture tests and 15 tensile test per material). The specimens were manufactured with three different raster orientations (0/90, 30/-60 and 45/-45), with the aim of evaluating the corresponding effect on the fracture behaviour. Thus, each raster orientation was covered with 8 fracture tests (4 per material) and 10 tensile tests, respectively. The three raster orientations are represented in Figure 1.

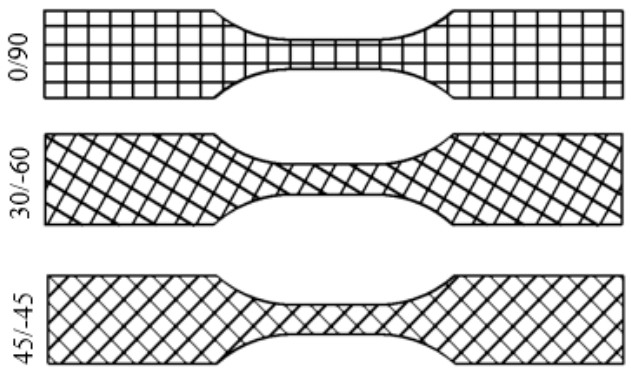

Fig. 1. Tensile specimen schematic with different raster orientations.

The fracture and tensile specimens were fabricated using a 3D printer (Prusa i3) by FDM, with the following printing parameters: nozzle diameter 0.4 mm; nozzle temperature 200 ºC; bed temperature 75 ºC; printing rate 30mm/s; infill level 100%; layer height 0.3 mm. A schematic of the tensile and fracture specimens is represented in Figure 2.

Tensile tests were performed in a servo-hydraulic testing machine (Servosis, Madrid, Spain) with a load capacity of 5kN. The displacement rate was fixed at 1 mm/mm, following ASTM638(2014). An axial extensometer (INSTRON, Norwood, MA, USA) was used to control the strain.

Fracture tests were performed on Single Edge Notched Bend (SNB) specimens. The crack-like defects were made by sawing a razor blade (following ASTM D6068, 2014). An electro-mechanical machine (Zwick-Roell BT1-FR2.ST5, Zwick-Roell, Ulm, Germany) with a load capacity of 2.5 kN was used. Again, the displacement rate was fixed at 1 mm/mm. The tests were carried out following ASTM D6068 (2014) because of the expected non-linear behaviour.

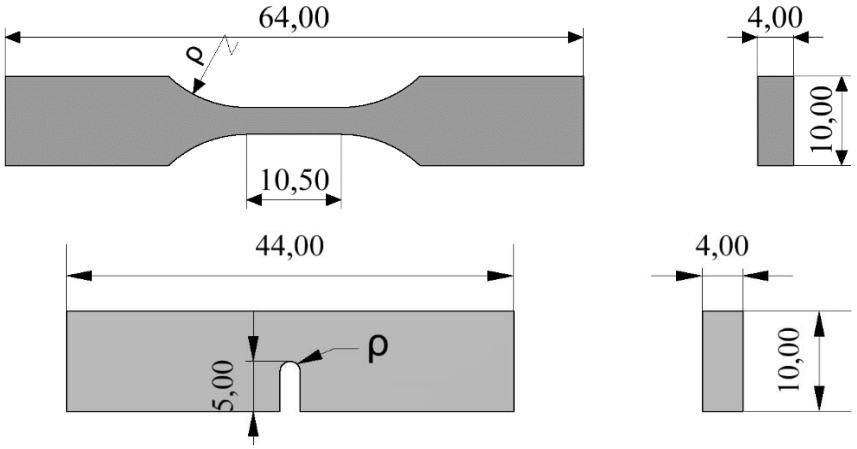

Fig. 2. Specimens dimensions used for the fracture and tensile tests respectively. ρ is assumed to be 0 mm (crack-like defects).

ASTM D6068 (2014) implies obtaining J_{mat} by using equation (1), with U being the area below the load-displacement curve, B being the thickness of the specimen (4 mm), W being the corresponding width (10 mm) and a_0 being the initial crack length. The coefficient η is equal to 2 in SENB specimens,

$$J_{mat} = \frac{\eta \cdot U}{B \cdot (W - a_0)} \tag{1}$$

Once J_{mat} is determined, the next step consists in obtaining the fracture toughness in stress intensity factor units (K_{mat}), applying equation (2). The Young´s modulus (E) is obtained from the tensile test, while υ refers to the Poisson modulus.

$$K_{mat} = \sqrt{\frac{J_{mat} \cdot E}{1 - \upsilon^2}} \tag{2}$$

Finally, the research work was completed with a Scanning Electron Microscopy (SEM) analysis of the fracture surfaces, with the goal of determining the relation between the experimental observations (i.e., fracture toughness results) and the corresponding fracture micromechanisms.

3. Results

The results obtained in the tensile tests are summarised in Table 1, with some of the tensile curves being shown in Fig. 3. The graphene addition has a clear effect on tensile properties, increasing the Young's modulus in all raster orientations and reducing the ductility of the material. This effect is not identical for each orientation: specimens with a raster orientation of 0/90 present an increase in the Young's modulus of +10%, while the ductility is reduced by 17%; for raster orientation 45/-45, the elastic modulus shows an increase of +44%, whereas ductility is reduced by 42%. The 30/-60 raster orientations shows intermediate results, with an increase of +22% in the Young´s modulus, and a 16% decrease in ductility.

The consequence of the raster orientation is also observable. The PLA behaviour becomes more ductile as the raster orientation gets closer to 45/-45, while 0/90 samples manufactured present the lowest ductility. This raster

orientation effect is less evident with the graphene addition, causing a homogenisation of the tensile properties.

Table 1 : Tensile properties of PLA and PLA-GRA. E: Young's modulus; ε: Strain under maximum load.

		PLA	PLA-GR	Graphene effect
E (MPa)	0/90	3769	4135	+10%
σ_u (MPa)		52,0	51,0	-1,9%
ε (%)		1,68	1,41	-16%
E (MPa)	30/-60	3313	4065	+23%
σ_u (MPa)		42,0	44,3	+5,4
ε (%)		1,94	1,64	-16%
E (MPa)	45/-45	2751	3972	+44%
σ_u (MPa)		41,1	49,0	+19,4
ε (%)		2,59	1,50	-42%

It can be observed (Figure 3) how the graphene addition causes a displacement of the original PLA curves to the left and upwards, implying, in general, an improvement of the ultimate tensile strength and a reduction in the strain under maximum load. However, the raster orientation causes the opposite effect, moving the curves to the right and downwards. Those results are similar to others found in the literature (e.g., Ayatollahi et al., 2020; Chieng et al., 2014).

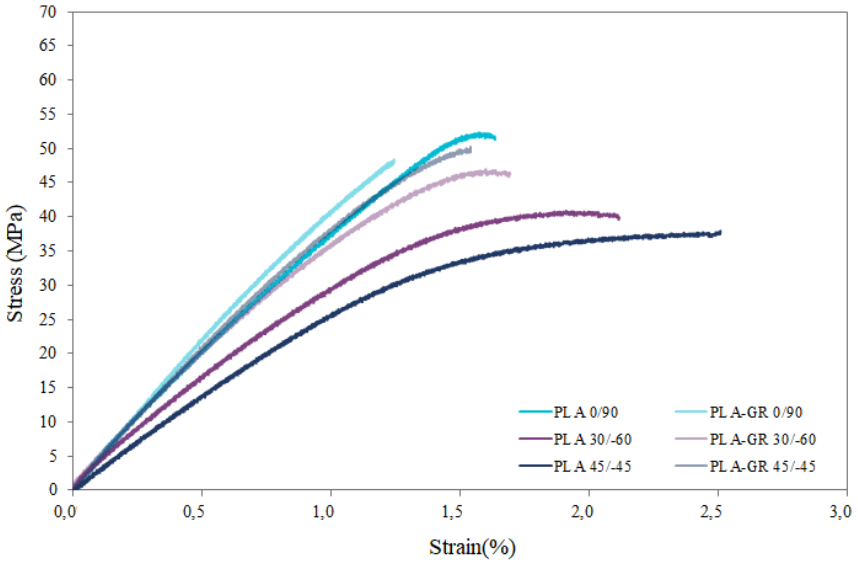

Fig. 3. Tensile curves per each raster orientation of PLA and PLA-GRA.

The fracture test results are gathered in Table 2 and Fig. 4. The graphene addition may have a significant effect on the fracture behaviour, but as occurred with the tensile properties, the intensity of this effect strongly depends on the raster orientation. Figure 4 shows the fracture toughness values for PLA and PLA-GR for each raster orientation, and it can be observed how graphene implies a negligible effect on raster orientation 0/90. However, raster orientation 30/-60 presents a 20% increase in the fracture toughness when adding 1 wt.% of graphene, and raster

orientation 45/-45 improves the toughness by 56%. Thus, raster orientation 45/-45 presents the lowest fracture resistance for the PLA material, and becomes the toughest material when adding the graphene.

This analysis implies that 3D printing at 0/90 should be avoided in the presence of graphene, because no improvement has been observed. However, the printing process can be performed with raster orientations such as 30/-60 or 45/-45, for which a significant enhancement of the fracture behaviour may be expected.

Finally, a SEM analysis was performed in order to evaluate the different fracture mechanisms. Two fracture surfaces have been analysed per raster orientation, one for PLA material and another one for PLA-GRA (see figures 5 and 6). In all cases, the specimens showed macro-porosity, which is common in additive manufacturing processes even for 100% infill level.

The addition of graphene produces a rough surface in PLA-GR specimens in the three raster orientations, while PLA samples always exhibit clear brittle micromechanisms. However, the roughness is much more significant in the samples fabricated at 45/-45, affecting the whole fracture surface. Raster orientation 0/90, however, only presents the change in fracture micromechanisms (from brittle surface to rough surface) in the filaments oriented in the perpendicular direction to the acting stresses (90° orientation), whereas the filaments oriented in the same direction as the acting stresses (0° orientation) remain brittle. Consequently, the variation in the observed fracture resistance is much more limited.

Table 2: Geometry and results of the fracture tests.

Material	Raster Orientation	Test	W (mm)	b (mm)	a_0 (mm)	K_{mat} (MPa·m$^{1/2}$)	K_{mat} avg. (MPa·m$^{1/2}$)
PLA	0/90	1	11,05	4,00	5,19	5,59	5,61
PLA	0/90	2	11,02	4,00	5,05	5,28	
PLA	0/90	3	11,12	4,00	5,15	5,89	
PLA	0/90	4	11,07	4,00	4,97	5,68	
PLA-GR	0/90	1	10,89	4,00	5,05	5,55	5,61
PLA-GR	0/90	2	10,90	4,00	5,02	5,45	
PLA-GR	0/90	3	10,73	4,00	5,29	5,95	
PLA-GR	0/90	4	10,84	4,00	5,06	5,50	
PLA	30/-60	1	10,92	4,00	5,42	5,76	5,76
PLA	30/-60	2	10,89	4,00	5,17	5,54	
PLA	30/-60	3	10,91	4,00	5,27	5,61	
PLA	30/-60	4	11,01	4,00	5,06	6,15	
PLA-GR	30/-60	1	11,02	4,00	5,05	7,06	6,92
PLA-GR	30/-60	2	11,06	4,00	5,00	7,16	
PLA-GR	30/-60	3	11,14	4,00	5,51	6,90	
PLA-GR	30/-60	4	11,00	4,00	5,44	6,55	
PLA	45/-45	1	10,92	4,00	5,42	4,97	4,59
PLA	45/-45	2	10,83	4,00	5,17	4,46	
PLA	45/-45	3	10,89	4,00	5,27	4,58	
PLA	45/-45	4	10,92	4,00	5,06	4,36	
PLA-GR	45/-45	1	11,08	4,00	5,05	7,58	7,20
PLA-GR	45/-45	2	11,09	4,00	5,00	7,38	
PLA-GR	45/-45	3	11,05	4,00	5,51	7,03	
PLA-GR	45/-45	4	10,83	4,00	5,44	6,79	

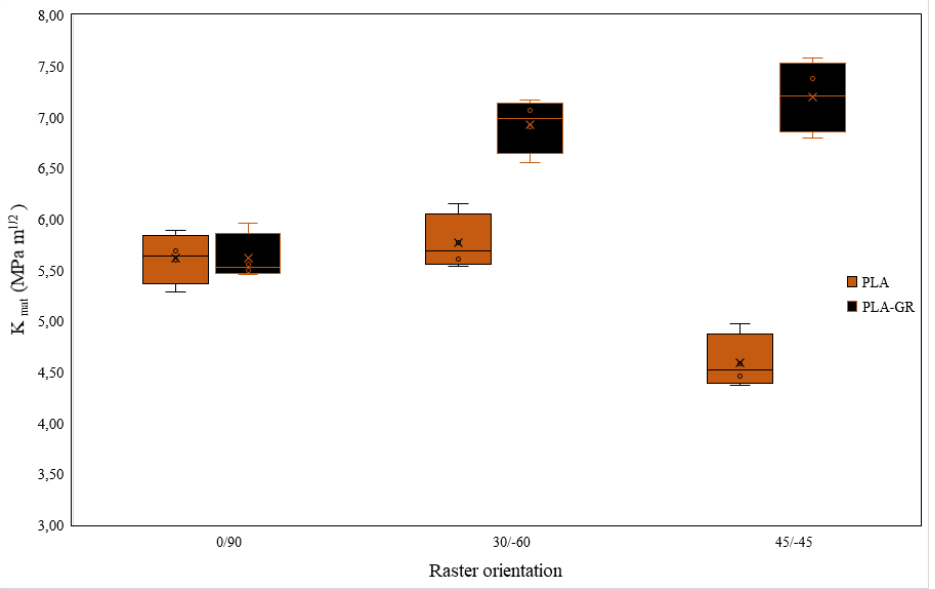

Fig. 4. Fracture toughness of PLA and PLA-GRA, for 0/90, 30/-60 and 45/-45 raster orientation.

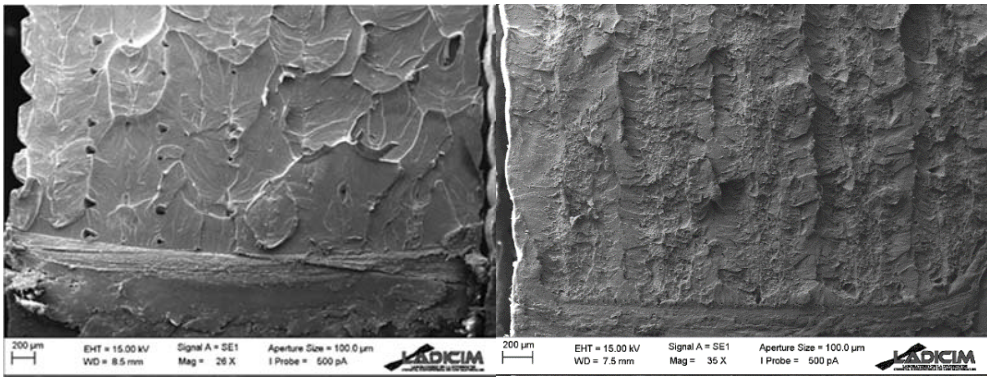

Fig. 5. SEM images obtained from 0/90 raster orientation. PLA (left); PLA-GR (right).

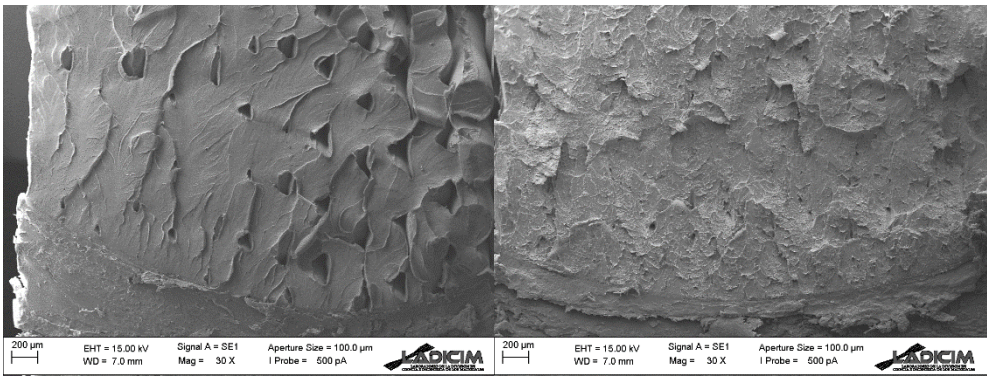

Fig. 6. SEM images from 45/-45 raster orientation. PLA (left); PLA-GR (right).

4. Conclusions

This paper evaluates the fracture behaviour of 3D-printed PLA and 3D-printed PLA reinforced with graphene. The experimental approach was composed of tensile and fracture tests that have been complemented with a SEM analysis of the fracture surfaces. The main conclusions are the following:

- The addition of graphene generates an enhancement in the tensile properties. The Young's modulus increases at the same time as the strain at rupture decreases. The effect on the ultimate tensile strength depends on the raster orientation: it is barely modified in 0/90 orientation, slightly increased in 30/-60 and significantly improved in 45/-45.
- Concerning the fracture behaviour of the PLA material, raster orientation 45/-45 presents the lowest fracture toughness.
- The fracture behaviour changes considerably when adding graphene (1 wt.%). Raster orientation 0/90 does not show any kind of improvement in the fracture toughness. On the contrary, a significant enhancement in the fracture resistance is observed in 30/-60 and, specially, 45/-45 raster orientations.
- The fracture behaviour evolution has been justified by the SEM analysis. When adding graphene, the fracture surface in 0/90 raster orientation remains similar to that observed in PLA in half of the filaments, limiting the evolution in the fracture toughness. However, 30/-60 and 45/-45 orientations present different (rougher) mechanisms in all the filaments when adding the reinforcement, with the corresponding increase in the fracture toughness.

Acknowledgments

The authors of this work would like to express their gratitude to the Spanish Ministry of Science and Innovation for the financial support of the project PGC2018-095400-B-I00 "Comportamiento en fractura de materiales compuestos nano-reforzados con defectos tipo entalla".

References

Afrose, M.F., Masood, S.H., Nikzad, M., Iovenitti, P., 2014. Effects of build orientations on tensile properties of PLA material processed by FDM. Adv. Mater. Res. 1044–1045, 31–34. https://doi.org/10.4028/www.scientific.net/AMR.1044-1045.31

ASTM D6068, 2014. ASTM D6068 " Standar method for determining J-R cuves of plastic materials."

ASTM D638-14, 2014. ASTM D638-14, Standard Test Method for Tensile Properties of Plastics. ASTM International, West Conshohocken, PA.

Ayatollahi, M.R., Nabavi-Kivi, A., Bahrami, B., Yazid Yahya, M., Khosravani, M.R., 2020. The influence of in-plane raster angle on tensile and fracture strengths of 3D-printed PLA specimens. Eng. Fract. Mech. 237, 107225. https://doi.org/10.1016/j.engfracmech.2020.107225

Bamiduro, O., Owolabi, G., Haile, M.A., Riddick, J.C., 2019. The influence of load direction, microstructure, raster orientation on the quasi-static response of fused deposition modeling ABS. Rapid Prototyp. J. 25, 462–472. https://doi.org/10.1108/RPJ-04-2018-0087

Caminero, M.Á., Chacón, J.M., García-Plaza, E., Núñez, P.J., Reverte, J.M., Becar, J.P., 2019. Additive manufacturing of PLA-based composites using fused filament fabrication: Effect of graphene nanoplatelet reinforcement on mechanical properties, dimensional accuracy and texture. Polymers (Basel). 11. https://doi.org/10.3390/polym11050799

Chieng, B.W., Ibrahim, N.A., Yunus, W.M.Z.W., Hussein, M.Z., 2014. Poly(lactic acid)/poly(ethylene glycol) polymer nanocomposites: Effects of graphene nanoplatelets. Polymers (Basel). 6, 93–104. https://doi.org/10.3390/polym6010093

Dwiyati, S.T., Kholil, A., Riyadi, R., Putra, S.E., 2019. Influence of layer thickness and 3D printing direction on tensile properties of ABS material. J. Phys. Conf. Ser. 1402. https://doi.org/10.1088/1742-6596/1402/6/066014

Fernandez-Vicente, M., Calle, W., Ferrandiz, S., Conejero, A., 2016. Effect of Infill Parameters on Tensile Mechanical Behavior in Desktop 3D Printing. 3D Print. Addit. Manuf. 3, 183–192. https://doi.org/10.1089/3dp.2015.0036

Jap, N.S.F., Pearce, G.M., Hellier, A.K., Russell, N., Parr, W.C., Walsh, W.R., 2019. The effect of raster orientation on the static and fatigue properties of filament deposited ABS polymer. Int. J. Fatigue 124, 328–337. https://doi.org/10.1016/j.ijfatigue.2019.02.042

Kiendl, J., Gao, C., 2020. Controlling toughness and strength of FDM 3D-printed PLA components through the raster layup. Compos. Part B Eng. 180, 107562. https://doi.org/10.1016/j.compositesb.2019.107562

Marconi, S., Alaimo, G., Mauri, V., Torre, M., Auricchio, F., 2018. Impact of graphene reinforcement on mechanical properties of PLA 3D printed materials. 2017 IEEE MTT-S Int. Microw. Work. Ser. Adv. Mater. Process. RF THz Appl. IMWS-AMP 2017 2018-Janua, 1–3. https://doi.org/10.1109/IMWS-AMP.2017.8247414

Rankouhi, B., Javadpour, S., Delfanian, F., Letcher, T., 2016. Failure Analysis and Mechanical Characterization of 3D Printed ABS With Respect to Layer Thickness and Orientation. J. Fail. Anal. Prev. 16, 467–481. https://doi.org/10.1007/s11668-016-0113-2

Rodríguez-Panes, A., Claver, J., Camacho, A.M., 2018. The influence of manufacturing parameters on the mechanical behaviour of PLA and

ABS pieces manufactured by FDM: A comparative analysis. Materials (Basel). 11. https://doi.org/10.3390/ma11081333
Samykano, M., Selvamani, S.K., Kadirgama, K., Ngui, W.K., Kanagaraj, G., Sudhakar, K., 2019. Mechanical property of FDM printed ABS: influence of printing parameters. Int. J. Adv. Manuf. Technol. 102, 2779–2796. https://doi.org/10.1007/s00170-019-03313-0
Wu, W., Geng, P., Li, G., Zhao, D., Zhang, H., Zhao, J., 2015. Influence of layer thickness and raster angle on the mechanical properties of 3D-printed PEEK and a comparative mechanical study between PEEK and ABS. Materials (Basel). 8, 5834–5846. https://doi.org/10.3390/ma8095271
Ziemian, C., Sharma, M., Ziemi, S., 2012. Anisotropic Mechanical Properties of ABS Parts Fabricated by Fused Deposition Modelling. Mech. Eng. https://doi.org/10.5772/34233